





HOPS/TMUB1 retains p53 in the cytoplasm and sustains p53-dependent mitochondrial apoptosis

Marilena Castelli^{1,†}, Danilo Piobbico^{1,†}, Martina Chiacchiaretta^{1,†}, Cinzia Brunacci¹, Stefania Pieroni¹, Daniela Bartoli^{1,†}, Marco Gargaro¹, Francesca Fallarino^{1,2}, Paolo Puccetti^{1,2} , Silvia Soddu³ , Maria Agnese Della-Fazia^{1,*,§}  & Giuseppe Servillo^{1,2,§,**} 

Abstract

Apoptotic signalling by p53 occurs at both transcriptional and non-transcriptional levels, as p53 may act as a direct apoptogenic stimulus via activation of the intrinsic mitochondrial pathway. HOPS is a highly conserved, ubiquitously expressed shuttling protein with an ubiquitin-like domain. We generated *Hops*^{-/-} mice and observed that they are viable with no apparent phenotypic defects. However, when treated with chemotherapeutic agents, *Hops*^{-/-} mice display a significant reduction in apoptosis, suggesting an impaired ability to respond to genotoxic stressors. We show that HOPS acts as a regulator of cytoplasmic p53 levels and function. By binding p53, HOPS inhibits p53 proteasomal degradation and favours p53 recruitment to mitochondria and apoptosis induction. By interfering with importin α , HOPS further increases p53 cytoplasmic levels. Thus, HOPS promotes the p53-dependent mitochondrial apoptosis pathway by preserving cytoplasmic p53 from both degradation and nuclear uptake.

Keywords apoptosis; HOPS; mitochondria; p53; TMUB1; ubiquitin like

Subject Categories Autophagy & Cell Death; Membranes & Trafficking

DOI 10.15252/embr.201948073 | Received 12 March 2019 | Revised 15 November 2019 | Accepted 2 December 2019 | Published online 23 December 2019

EMBO Reports (2020) 21: e48073

Introduction

Hepatocyte odd protein shuttling (HOPS), also known as transmembrane and ubiquitin-like protein-1 (TMUB1)—hereafter referred to as HOPS—is encoded by a gene identified via screening of the proliferative process in regenerating liver [1–4]. *Hops* codifies three different isoforms. The long isoform (lHOPS) corresponds to the full-length mRNA, the short isoform (sHOPS) starts from an

alternative methionine sited at Aa 55 and a third, intermediate molecular-weight isoform (iHOPS) derives from a RIP (regulated intramembrane protease) N-terminal cleavage sited at Aa 30 [2]. Though ubiquitous, HOPS is abundantly expressed in the brain, where it localizes in the synaptosomal membranous compartment [3]. HOPS deficiency in knockout mice has been found to be associated with behavioural changes, including nocturnal hyperactivity [5]. HOPS shuttles between nucleus and cytoplasm, in a cell cycle-dependent fashion, and it presents an ubiquitin-like (UBL) domain, three transmembrane domains, and proline- and leucine-rich domains [2]. In response to growth factors or oxidative stress, HOPS migrates from the nucleus to the cytoplasm through the activity of CRM1 [1], while in resting cells, HOPS accumulates in the nucleus and causes cell cycle arrest in G₀/G₁ [1]. HOPS knockdown has been shown to cause centrosome amplification, micronuclei formation and multinucleated cells [6], supporting role(s) in centrosomal assembly and maintenance, mitotic spindle organization, and cell division. In previous studies, we showed that HOPS controls the stability of the tumour suppressor p19^{Arf} [7]. In particular, HOPS, NPM1 and p19^{Arf} form a trimeric complex, in which HOPS acts both as a bridge for NPM1 to stabilize p19^{Arf} and as a direct controller of p19^{Arf} stability. In this context, HOPS overexpression increases p19^{Arf} half-life and, in turn, enhances p53 level [7,8].

The *TP53* is a key tumour suppressor gene, and its p53-encoded protein plays a pivotal role in the global biology of the cell [9–11]. p53 controls important cellular processes, such as DNA repair, apoptosis, metabolism, stemness, development and inflammation [12–16]. Cancer development and progression is causally linked to p53 modifications. More than 50% of human cancers show a mutation or deletion in the *TP53* gene, while anomalies in p53 regulator activity are found in most of the remaining 50% [17–19]. Evasion of apoptosis is a main cancer hallmark [20], and apoptosis induction is critical for p53 tumour suppressor activity *in vivo* [21–23]. Recent studies highlighted the important role of cytoplasmic p53, which acts as an inducer of mitochondrial apoptosis as a consequence of

¹ Department of Experimental Medicine, University of Perugia, Perugia, Italy

² Centro Universitario di Ricerca sulla Genomica Funzionale (C.U.R.Ge.F.), University of Perugia, Perugia, Italy

³ Unit of Cellular Networks and Molecular Therapeutic Targets, IRCCS – Regina Elena National Cancer Institute, Rome, Italy

*Corresponding author. Tel: +390755858111; E-mail: mariaagnese.dellafazia@unipg.it

**Corresponding author. Tel: +390755858110; E-mail: giuseppe.servillo@unipg.it

[†]Daniela Bartoli Deceased, 02 September 2019

[‡]These authors contributed equally to this work

[§]These authors contributed equally to this work as senior authors

its accumulation [24–26]. p53 accumulation outside of the nuclear compartment is an essential step in determining both mitochondrial apoptosis and autophagy [24,27]. The overall mechanisms controlling p53 homeostasis and/or accumulation in the cytoplasm are characterized by considerable complexity. Under normal conditions, newly synthesized p53 accumulates in the nucleus, being present in the cytoplasm only in a discreet amount, strictly controlled by p53 ubiquitination and proteasomal degradation. In response to an apoptogenic stressor, a significant amount of p53 accumulates in the cytoplasm, where it engages in apoptotic events by directly acting on mitochondria [25]. However, the cytoplasmic mechanism preserving newly recruited p53 from degradation and nuclear uptake is unclear.

To gain insight into the overall functioning of HOPS, we generated *Hops*^{-/-} mice and analysed the animals by challenge with panoply of stimuli. One major effect was the impaired ability of *Hops*^{-/-} mice to mount an apoptotic response to genotoxic stressors. In particular, we found that *Hops*^{-/-} mice do not undergo p53-driven mitochondrial apoptosis. Mechanistically, we showed that HOPS directly interacts with p53 and inhibits its ubiquitination/degradation through the UBL domain, in an ARF-independent manner. In addition, HOPS retains p53 in the cytoplasm, boosting its mitochondrial-related apoptotic response, by opposing the p53 nuclear import via competition with importin α .

Results

Hops^{-/-} mice are resistant to etoposide-induced apoptosis

To gain insight into HOPS functions, a *Hops*^{-/-} mouse line was generated using homologous recombination. *Hops*^{-/-} deleted ES cells were purchased by Knockout Mouse Project (KOMP). The *Hops*^{-/-} cells were obtained by removing 1,027 bps in chromosome 5 (23,952,734–23,951,708), a sequence spanning the entire *Hops*-coding region (Fig 1A). Embryonic stem cells on a C57BL/6NTac background were transfected with the knockout gene construct and microinjected into blastocyst to obtain chimera, allowing for germ-line transmission of the mutant allele. The resulting chimera was mated to C57BL/6 females to generate mice that were heterozygous (*Hops*^{+/-}) for the exon 2–3 deletion. Heterozygous mice were intercrossed with homozygous (*Hops*^{-/-}) counterparts, yielding a *Hops*^{-/-} mouse line. To obtain the *Hops*^{-/-} mouse line, heterozygous vs homozygous mice were intercrossed, rather than homozygous by themselves, since knockout mice show a reduced ability to generate offspring. Successful gene knockout was confirmed by PCR genotyping and by assessing *Hops* mRNA and protein levels (Fig 1B).

Hepatocyte odd protein shuttling did not appear to be required for normal development even if the nullizygous mice were born with a slightly reduced Mendelian frequency (Fig 1C). Mice of both genders were viable and did not manifest evident abnormalities when maintained under normal farming conditions. However, when mice were challenged with stressors, such as induction of DNA damage by etoposide treatment, significant resistance to apoptosis was observed in the *Hops*^{-/-} compared to *Hops*^{+/+} mice. In particular, *Hops*^{+/+} and *Hops*^{-/-} littermates were treated with etoposide and their thymus, spleen and testis, analysed at 2 and 4 h of treatment, by cleaved caspase-3 immunofluorescence (IF) and TUNEL

(Terminal deoxynucleotidyl transferase dUTP Nick End Labeling) staining; liver was utilized as negative control [28]. We observed a remarkable reduction in apoptosis levels in tissues from *Hops*^{-/-} mice relative to their HOPS-competent counterparts. In *Hops*^{+/+} mice, thymus, spleen and testis showed a large number of cleaved caspase-3 positive cells, in accordance with previous results [28]. Instead, rare cells were found positive in *Hops*^{-/-} mice (Fig 2A and Appendix Fig S1). Similar results were obtained by TUNEL assay (Appendix Fig S2). In these conditions, no apoptotic effects were observed in the livers from mice of both genotypes (Fig 2A and Appendix Figs S1D and S2D).

HOPS deficiency impairs p53 activation

p53 is a key mediator of apoptosis in DNA damage response [10,21,29,30]. Thus, we examined the pattern of p53 expression by Western blotting (WB) in *Hops*^{+/+} and *Hops*^{-/-} mice in response to etoposide. Consistent with previous reports [28], increased p53 expression in the thymus, spleen and testis was observed at 2 and 4 h of etoposide treatment in *Hops*^{+/+} mice. In contrast, no p53 induction was detected in *Hops*^{-/-} mice. No relevant activation was observed in etoposide-treated livers employed as negative control (Fig 2B). Indeed, in the tissues of *Hops*^{-/-} mice and in MEF *Hops*^{-/-} examined by WB, we found that p53 protein level is higher with respect to *Hops*^{+/+}. To further assess the functional relationship between HOPS and p53 in apoptosis induction, thymocytes from *Hops*^{+/+} and *Hops*^{-/-} mice were treated with dexamethasone, a p53-independent apoptogenic stimulus. As assessed by FACS analysis after 8 h of dexamethasone treatment [31], *Hops*^{+/+} and *Hops*^{-/-} thymocytes showed similar levels of apoptosis (Figs 3A and EV1A), indicating that *Hops*^{-/-} cells are not constitutively resistant to any type of apoptosis.

Next, we examined the *in vitro* induction of DNA damage-induced apoptosis in mouse embryo fibroblasts (MEFs). We treated *Hops*^{+/+} and *Hops*^{-/-} MEFs with etoposide or camptothecin for 6 h. FACS analysis revealed remarkably reduced apoptosis levels in *Hops*^{-/-} MEFs relative to *Hops*^{+/+} control cells with both drugs (Figs 3B and EV1B and C). To substantiate the role of HOPS in apoptosis, we analysed the effect of the overexpression of HOPS in MEF *Hops*^{+/+}. We transfected the MEF *Hops*^{+/+} with EGFP-N1-Hops and then we analysed the apoptosis in EGFP-Hops positive cells. The results showed that more of 60% of EGFP-Hops positive cells result apoptotic respect to the relative control (Fig 3C). Moreover, same experiments performed in MEF *Hops*^{-/-} showed, also in these case, similar percentage of apoptotic cells (Fig 3C). WB analyses of treated MEFs showed that p53 expression is less increased in the drug-treated *Hops*^{-/-} MEFs compared to the *Hops*^{+/+} counterparts (Figs 3D and EV1D).

Taken together, these data suggested that lack of HOPS makes cells more resistant to DNA damage-induced apoptosis and its overexpression activates apoptosis in MEFs.

HOPS controls p53 stability by impairing its MDM2-mediated ubiquitination

Hepatocyte odd protein shuttling has been shown to regulate ARF protein levels which, in turn, might increase p53 protein stability [7]. Thus, we asked whether HOPS might affect p53 half-life in an

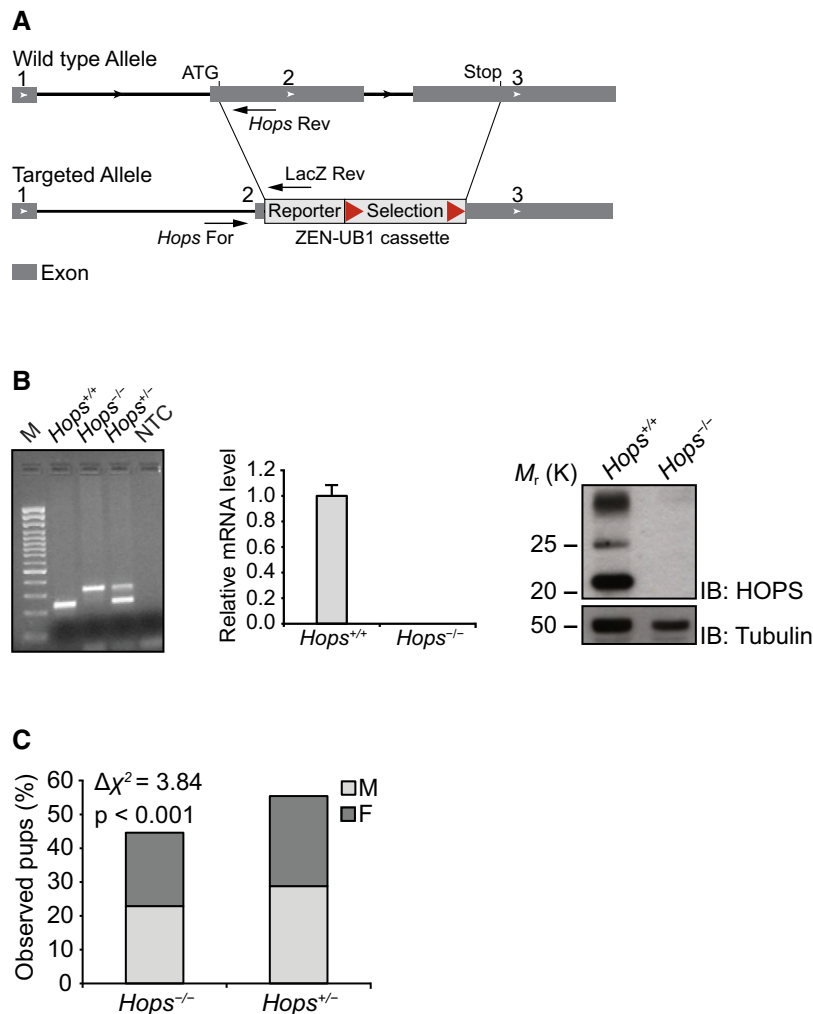


Figure 1. Generation of *Hops*^{-/-} mouse.

A Schematic diagram of gene targeting of *Hops* locus. Targeting vector containing lacZ and a ZEN-UB1 cassette was inserted into HOPS gene between exons 2 and 3, flanking with 2 kb 5'—homology and 2 kb 3'—homology.

B *Hops*^{-/-} mouse genotyping and protein expression. Genotyping by PCR using genomic DNA showed a 242-bp band for wild-type (*Hops*^{+/+}) allele and a 331-bp band for mutant (*Hops*^{-/-}) allele. NTC is null template control (left panel). Genotyping by real-time PCR confirmed the absence of *Hops* mRNA in *Hops*^{-/-} mice (middle panel). Protein extracts from *Hops*^{+/+} and *Hops*^{-/-} MEFs were analysed by Western blot using anti-HOPS antibody and anti- α -tubulin antibody as loading control (right panel).

C Offspring distribution. Different HOPS genotypes at weaning age (approximately postnatal day 21) from crosses between homozygous knockout mice males and heterozygous females ($n = 1,525$ pups).

Data information: In (B), data are presented as mean \pm SD. In (C), the chi-square test was performed to determine significant differences between the expected and observed ratios of *Hops*^{-/-} to *Hops*^{+/+} mice. $P < 0.001$, by two-tailed Student's *t*-test.

ARF-dependent manner. WB analyses of *Hops*^{+/+} and *Hops*^{-/-} MEFs treated with cycloheximide clearly showed significantly lower p53 half-life in the *Hops*-defective cells, while rescue of HOPS by its ectopic expression in *Hops*^{-/-} MEFs significantly increased the p53 half-life (Fig 4A). Next, *p19*^{Arf}^{-/-} MEFs and human ARF-deficient A549 cells carrying endogenous wild-type p53 were transfected with HOPS or empty vector as a control, and treated with cycloheximide. In both cell types, WB of p53 performed at different time points clearly indicated higher half-life values for p53 in the cells overexpressing HOPS (Figs 4B and EV2A), indicating that ARF is dispensable for HOPS-induced increased of p53 stability.

Thus, we investigated whether HOPS preserves p53 from ubiquitination and proteasomal degradation through its UBL domain in an MDM2-dependent manner. Two different HOPS mutants were generated. The last glycine of the UBL domain at position 176, necessary for isopeptide bond, was replaced with alanine (HOPS-G176A); as a control, a lysine in the UBL domain at position 129 was likewise replaced (HOPS-K129A). Ubiquitination experiments were performed in the p53-null H1299 cells. Cells transfected with ubiquitin, p53 and MDM2 were further transfected with wild-type HOPS or either of its mutants, HOPS-G176A and HOPS-K129A. Cells were then treated with the proteasome inhibitor MG132.

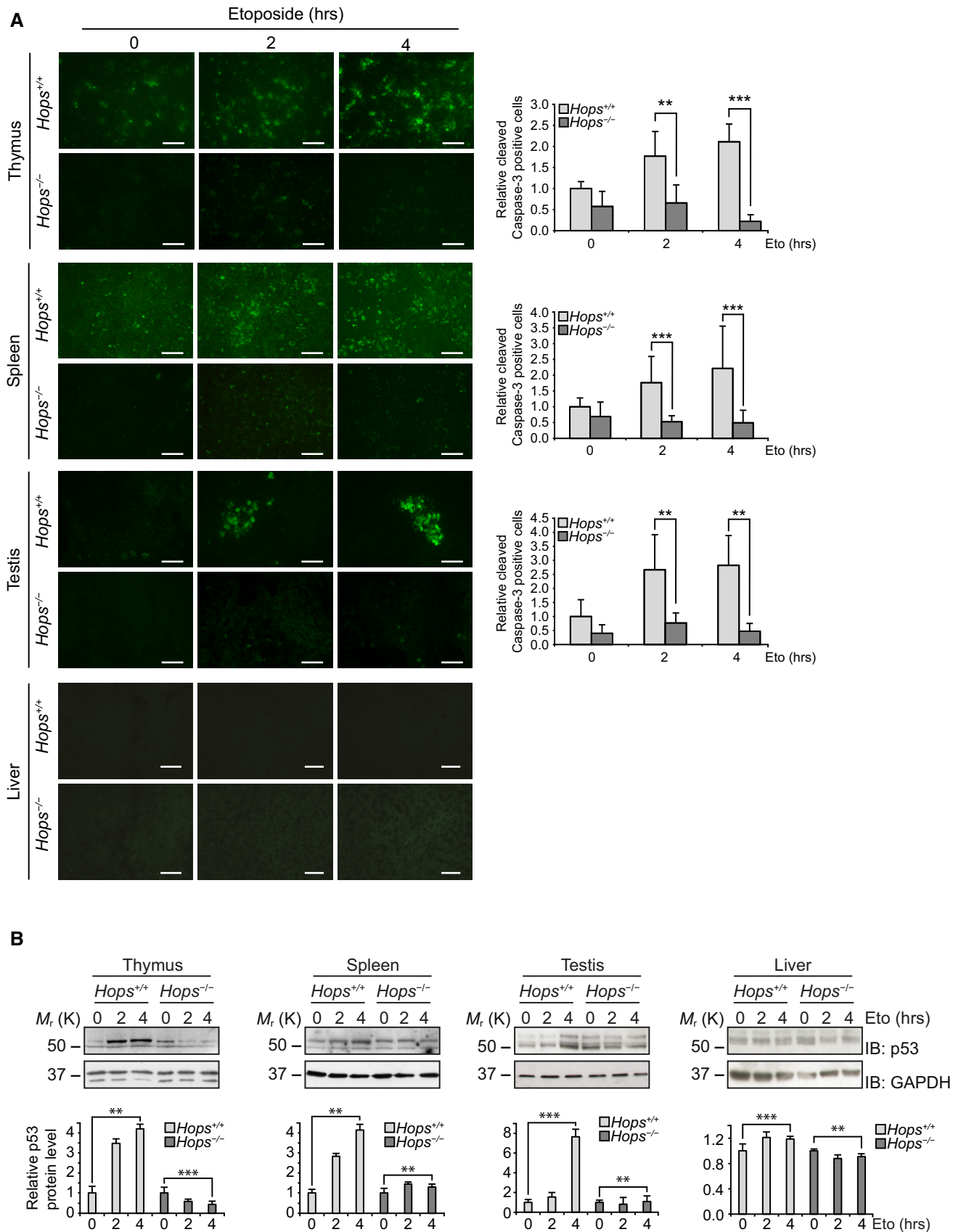


Figure 2.

Figure 2. *Hops*^{-/-} mice resistance to apoptosis.

A Reduced caspase-3 activation in *Hops*^{-/-} mice upon apoptotic stimulus. *Hops*^{+/+} and *Hops*^{-/-} mice were treated with etoposide for the indicated times, and thymus, spleen, testis and liver were harvested and Tissue-Tek® O.C.T. embedded. Sections were immunostained with anti-cleaved caspase-3 antibody followed by appropriate secondary antibody labelling (green). The graphs display the relative positive cells number. Scale bars, 10 μm. Cleaved caspase-3 and DAPI staining merged images are shown in Appendix Fig S1A–D.

B HOPS affects p53 increase after stress *in vivo*. Whole-cell homogenates from organs were immediately prepared and immunoblotted with antibodies to detect p53 and GAPDH. The p53 levels were semi-quantified using GAPDH as loading control, and relative p53 levels at time 0 were assumed as 1.

Data information: All the experiments were performed three times in three different mice per condition, and a representative example is shown. In (A, B), data are presented as mean ± SD. ***P* < 0.01; ****P* < 0.001, by two-tailed Student's *t*-test.

Ubiquitinated proteins were subjected to pull-down with Ni²⁺-NTA resin and analysed by WB. Wild-type HOPS overexpression drastically reduced MDM2-mediated p53 ubiquitination, while no effect was observed by co-transfection of the HOPS-G176A mutant (Fig 4C). Much like the wild-type protein, the HOPS-K129A mutant inhibited MDM2-mediated ubiquitination of p53 (Fig 4C). Thus, a functional UBL domain is critical for HOPS control of p53 ubiquitination.

We next analysed the rate of p53 ubiquitination in *Hops*^{+/+} and *Hops*^{-/-} MEFs transfected with ubiquitin, p53, and MDM2, and treated with MG132. Higher levels of p53 ubiquitination were observed in the *Hops*^{-/-} MEFs compared with the *Hops*^{+/+} (Fig 4D). In addition, ectopic expression of wild-type HOPS in *Hops*^{-/-} MEFs decreased p53 ubiquitin levels, while the HOPS-G176A mutant failed to restrain p53 ubiquitination (Fig 4D). The latter finding was in line with the failure of HOPS-G176A to prolong p53 half-life in *Hops*^{-/-} MEFs (Fig 4E). As showed for ARF-independent control of p53 half-life, ubiquitination studies using ARF-deficient A549 cells showed that HOPS binds p53 (Fig EV2B) and reduces p53 ubiquitination via MDM2 in ARF-independent manner (Fig EV2C).

Overall, these data indicate that HOPS contributes to p53 protein stability acting as a regulator of its MDM2-mediated ubiquitination.

HOPS and p53 interact in ARF- and MDM2-independent manner

To evaluate whether HOPS and p53 belong to the same protein complexes, co-immunoprecipitation (co-IP) assays were performed in p53-null H1299 cells transfected with p53 and in RKO cells, constitutively expressing HOPS and p53. As shown in Fig EV3A and B, HOPS and p53 proteins were found in both co-IP settings. Comparable HOPS and p53 co-IP were obtained in *p19*^{Arf}^{-/-} MEFs and A549 cells, further supporting ARF independency (Figs EV2B and EV3C). In addition, HOPS and p53 co-IP also occurred in the absence of MDM2, as assessed in *p53-Mdm2* double knockout MEFs upon HOPS and p53 co-expression (Fig EV3D).

Next, *in vitro* binding assays performed with purified proteins showed a direct protein–protein interaction between p53 and HOPS (Fig EV3E). IF analysis showed co-localization of the two endogenous proteins (Fig EV3F).

Finally, to characterize the p53 protein domain(s) involved in HOPS binding, co-IP assays were performed in H1299 cells transfected with *Hops* cDNA and myc-tagged p53 wild-type or deleted forms. The N-terminal activation domain (TAD) alone was unable to bind HOPS, while the other two main domains (the DNA binding domain, DBD, and the C-terminal domain, CTD) maintained their capacity to immunoprecipitate HOPS (Fig EV3G). These results

indicate that the binding site for HOPS excludes the TAD which, in turn, is required for the p53 binding with MDM2 [32].

HOPS promotes mitochondrial accumulation of p53

In response to apoptotic signalling, a fraction of p53 rapidly moves from the nucleus to the cytoplasm through the export factor CRM1/exportin-1 [24,33], being the cytoplasmic p53 a major source of mitochondrial p53 [24,25]. HOPS is a shuttling protein that migrates from the nucleus to the cytoplasm through CRM1 [1]. Thus, we evaluated whether HOPS might contribute to p53 cytoplasmic stabilization and mitochondrial accumulation. First, the effect of etoposide treatment on HOPS localization and p53 binding was assessed by IF and biochemical analyses in RKO cells. The interaction between HOPS and p53 was quantified using a Duolink® proximity ligation assay (PLA). Proximity ligation assay allows *in situ* detection of endogenous proteins and protein interactions with high specificity and sensitivity. Treatment with etoposide dramatically increased the association between the two proteins. We observed that, after etoposide treatment, a fraction of p53 migrates from the nucleus to the cytoplasm (Figs 5A and EV3F) and its binding with HOPS is enhanced at 2 and 4 h of treatment (Fig 5A). Proximity ligation assay revealed that the vast majority of the HOPS-p53 interaction was located in the cytoplasm (Fig 5A). These results have been confirmed by WB analysis, which demonstrated an enhanced HOPS-p53 binding in the cytoplasm (Fig 5B and C) and nuclei (Appendix Fig S3).

Because cytoplasmic p53 can localize at mitochondria, we asked whether also HOPS localizes and accumulates with p53 in these organelles. MitoTracker™ assay performed in RKO cells showed a clear localization of HOPS in mitochondria (Fig 6A), which was confirmed by WB of RKO mitochondria extracts (Fig 6B). Evaluation of the kinetics of p53 and HOPS accumulation in mitochondria at different times of etoposide treatment showed an accumulation of both proteins (Fig 6C). Similar results were obtained in A549 cells (Fig EV4A). In addition, HOPS-p53 co-IP experiments on mitochondrial extracts confirmed the co-localization of the two proteins in the organelles and their increased binding after etoposide treatment (Figs 6D and EV4B).

To evaluate whether HOPS is involved in p53 mitochondrial recruitment and function, we analysed the presence of mitochondrial p53 in tissues from *Hops*^{+/+} and *Hops*^{-/-} mice treated with etoposide. Mitochondria from thymus, spleen and testis were isolated at 2 and 4 h of treatment, and p53 mitochondrial translocation was assessed by WB analysis. In accordance with previous observations [28], a marked accumulation of p53 was observed in the mitochondria from thymus, spleen and testis of *Hops*^{+/+} mice

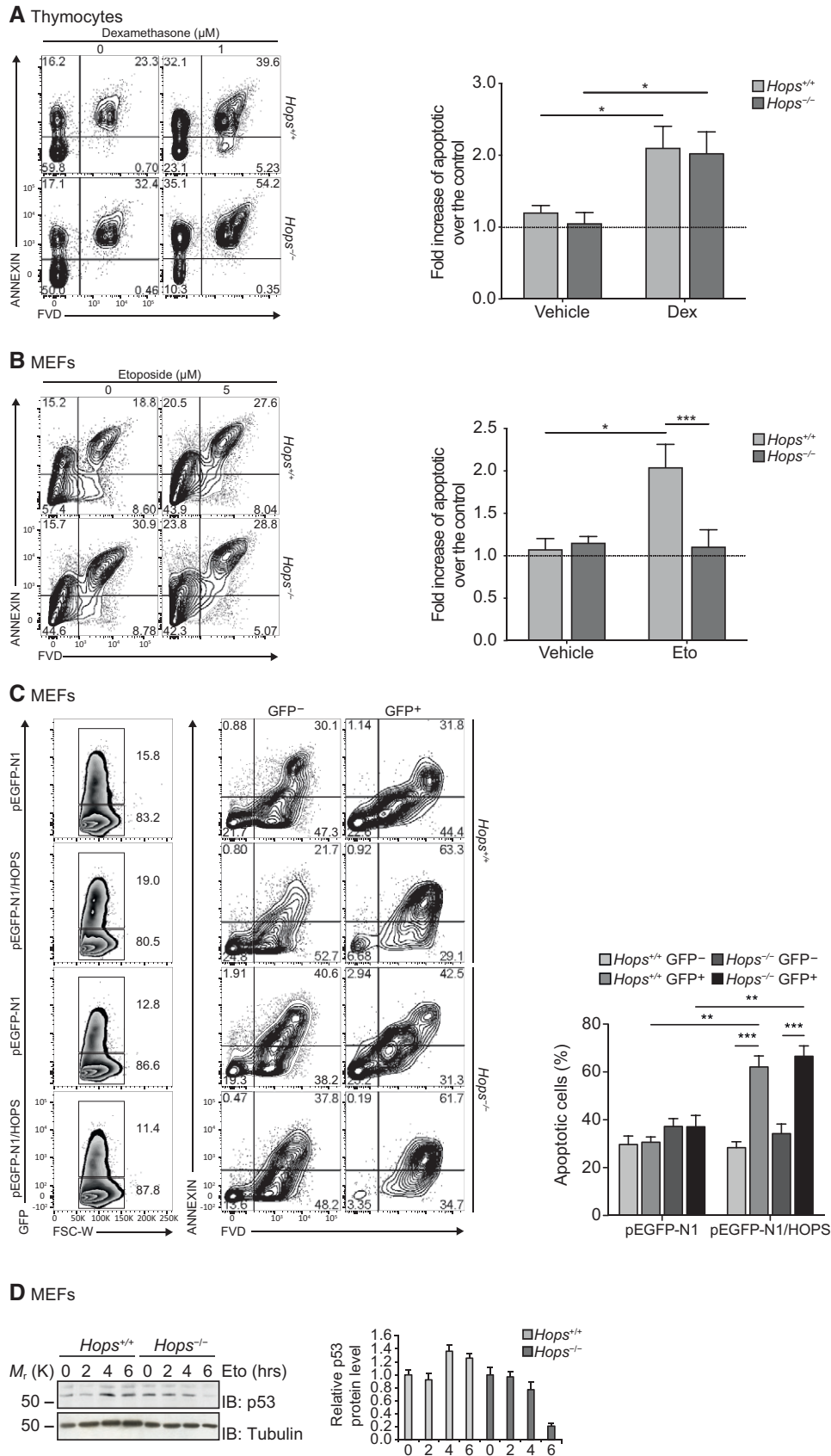


Figure 3.

Figure 3. HOPS acts on apoptosis induction.

- A Thymocytes from *Hops*^{+/+} and *Hops*^{-/-} mice were treated with dexamethasone (Dex), and the apoptotic cells were measured by flow cytometry. The flow cytometry analysis plots are shown on the left and the data represented as a histogram on the right.
- B HOPS was pivotal for apoptosis induction. *Hops*^{+/+} and *Hops*^{-/-} MEFs were subjected to etoposide (Eto), and apoptosis was analysed by flow cytometry (left) and showed as a graph (right).
- C HOPS overexpression in MEFs promotes apoptosis. *Hops*^{+/+} and *Hops*^{-/-} MEFs were transiently transfected with an empty vector (pEGFP-N1) or with a *Hops* encoding vector (pEGFP-N1-*Hops*). The apoptotic cells were measured by flow cytometry (left) on the GFP-positive and GFP-negative populations and showed as a graph (right).
- D HOPS affects p53 levels following stress *in vitro*. *Hops*^{+/+} and *Hops*^{-/-} MEFs were treated with etoposide and harvested at the indicated time points. The p53 protein levels were semi-quantified using α -tubulin as loading control, and relative p53 levels at 0 μ M dosage were assumed as 1.

Data information: The experiments were performed three times in primary cells from three different mice per condition. The experiments in MEFs were performed three times. Representative panels are shown. In (A–C), data are presented as mean \pm SD. **P* < 0.05; ***P* < 0.01; ****P* < 0.001, by two-tailed Student's *t*-test.

treated with the drug; no such effect was observed in *Hops*^{-/-} tissues (Fig 6E). Parallel experiments were conducted *in vitro*, by etoposide treatment of thymocytes and splenocytes isolated from *Hops*^{+/+} and *Hops*^{-/-} mice. A lower mitochondrial accumulation of p53 (Fig EV4C) and higher cell viability (Fig EV4D) was observed upon etoposide treatment in HOPS-deficient cells compared with the *Hops*^{+/+} counterparts.

Next, we assessed the mitochondrial membrane potential ($\Delta\Psi_m$) in *Hops*^{+/+} and *Hops*^{-/-} MEFs after etoposide treatment by using JC-1 dye. JC-1 dye accumulates in mitochondria and is currently used as a fluorescent marker of mitochondrial membrane potential variations as a green to red emission shift. We observed a clear reduction in the change of $\Delta\Psi_m$ in *Hops*^{-/-} MEFs with respect to *Hops*^{+/+} cells after the apoptotic stimulus (Fig 6F). Similar results were obtained by analysing thymocytes explanted from *Hops*^{+/+} and *Hops*^{-/-} mice (Fig EV4E). Indeed, the results obtained of analysis of membrane potential of mitochondria were confirmed by performing similar experiments with DiOC6(3) (Fig EV4F). DiOC6 (3) (3,3'-dihexyloxycarbocyanine iodide) is a cell-permeant, green-fluorescent, lipophilic dye applied to monitor the mitochondrial membrane potential by flow cytometry since it accumulates in mitochondria due to their negative potential.

To evaluate whether HOPS deficiency might *per se* affect mitochondrial function or involve p53 activity, we measured the mitochondrial outer membrane permeability (MOMP) by recording cytochrome c release of isolated mitochondria from *Hops*^{+/+} and *Hops*^{-/-} MEFs after the addition of recombinant p53. No significant differences in cytochrome c release were detected between mitochondria isolated from *Hops*^{+/+} and *Hops*^{-/-} MEFs (Fig 6G)

indicating that no intrinsic defects occur in the mitochondrial response of HOPS-deficient mice. These results support a role of HOPS in p53 accumulation, an event upstream of MOMP and a direct consequence of the HOPS-induced restraint of p53 cytoplasmic degradation.

Taken together, these data show that HOPS contributes to the mitochondrial programme of p53 in response to apoptogenic stimuli.

HOPS enforces cytoplasmic accumulation of p53 by impairing its nuclear import

Here we showed that, after etoposide treatment, HOPS binds and stabilizes p53 and drives it to mitochondria to allow p53-mediated apoptosis; however, a question remains open. How does HOPS, by binding p53 in the cytoplasm, hinder the return of p53 to the nucleus and favour p53-dependent mitochondrial apoptosis? Previous studies performed on p53 stabilization and localization have assessed that p53 ubiquitination occurs mainly in the cytoplasm. Moreover, the cytoplasmic pool of p53 requires its NLS region and depends on the importin α family, whose activity facilitates p53 import into the nucleus [34].

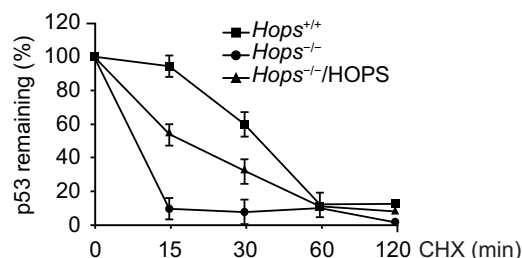
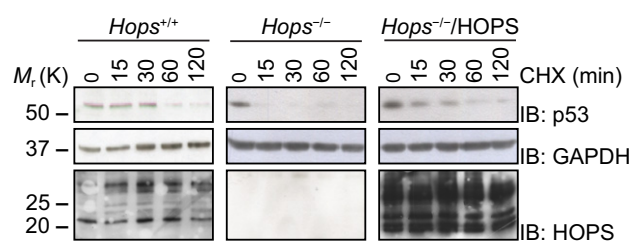
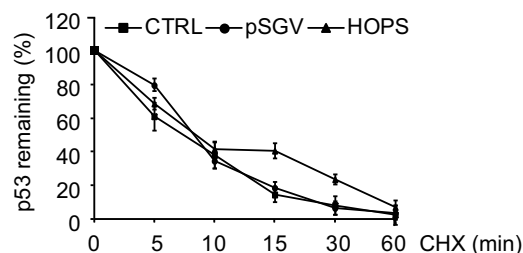
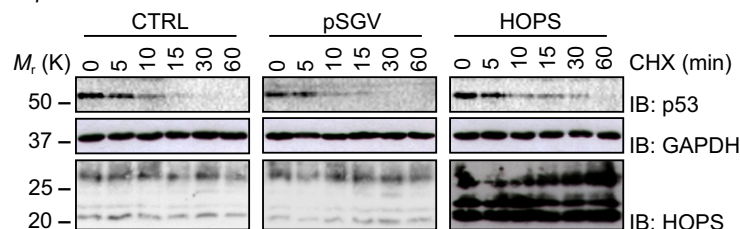
We found that HOPS binds p53 outside the TD required for the MDM2 interaction; thus, we asked whether HOPS might interact with the p53 NLS region and affect its nuclear import. First, we evaluated whether cytoplasmic p53 accumulates in RKO cells upon HOPS overexpression. Compared to control, the fraction of cells positive for cytoplasmic p53 was remarkably increased in the HOPS-transfected cells, as assessed by IF (Fig 7A) and WB (Fig 7B)

Figure 4. HOPS role in p53 stability and p53 ubiquitination.

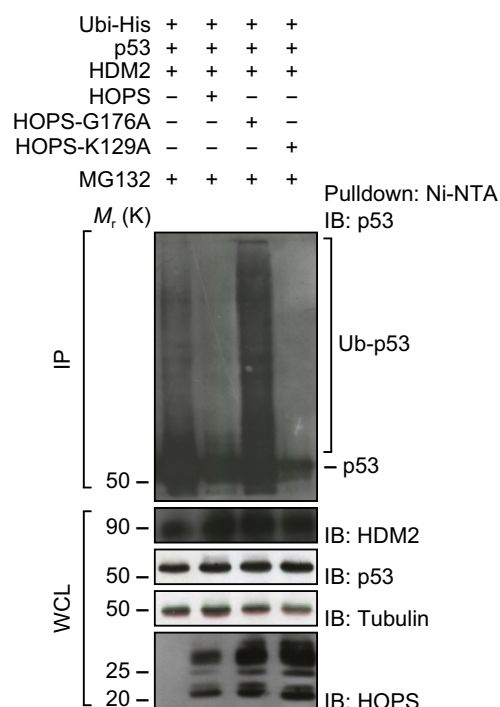
- A HOPS loss and p53 half-life. *Hops*^{+/+} and *Hops*^{-/-} MEFs untransfected or transfected with HOPS were analysed by immunoblotting following cycloheximide treatment for the indicated time (left panel). The p53 protein levels were semi-quantified using GAPDH as loading control, and relative p53 levels at time 0 were assumed as 100% (right panel).
- B p19^{Arf}-independent HOPS control of p53 half-life. p19^{Arf}^{-/-} MEFs untransfected (CTRL), transfected with empty vector (pSGV) or HOPS were treated with cycloheximide for the indicated times and subjected to immunoblot analysis with anti-p53, anti-HOPS and anti-GAPDH antibodies (left panel). The p53 protein levels were semi-quantified as above (right panel).
- C HOPS and p53 ubiquitination. p53, HDM2 and His-tagged ubiquitin were co-expressed in H1299 cells with HOPS or HOPS-G176A or HOPS-K126A mutants and treated with MG132. p53 ubiquitination rate was evaluated by elution using Ni²⁺-NTA His-bind resin followed by immunoblotting with anti-p53 and the indicated antibodies.
- D HOPS depletion and HOPS-G176A mutant affect p53 ubiquitination. *Hops*^{+/+} and *Hops*^{-/-} MEFs untransfected and *Hops*^{-/-} MEFs transfected with HOPS or HOPS-G176A mutant were co-expressed with p53, HDM2 and His-tagged ubiquitin. Cells were treated with MG132, and the ubiquitinated p53 fraction was recovered as above. Immunodetection of ubiquitinated p53 was performed using anti-p53 antibody, and the samples were tested with the indicated antibodies.
- E HOPS-G176A mutant ability to stabilize p53. *Hops*^{-/-} MEFs were transfected with HOPS-G176A, subjected to cycloheximide treatment for the indicated times and analysed by immunoblotting using the indicated antibodies.

Data information: All the experiments in MEFs were performed three times. Representative panels are shown. In (A, B), data are presented as mean \pm SD.

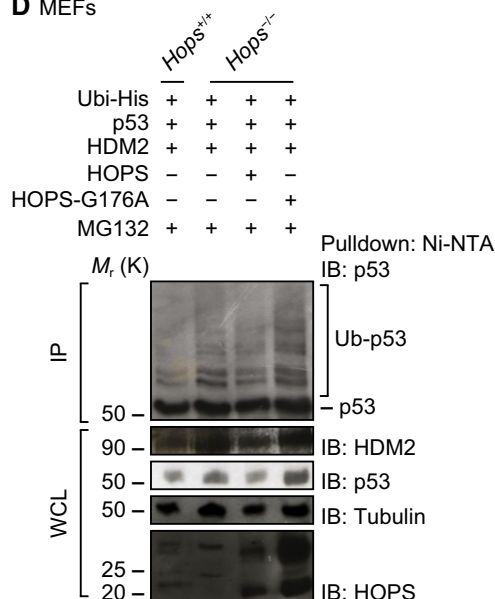
A MEFs

B *p19*^{Arf}^{-/-} MEFs

C H1299



D MEFs



E MEFs

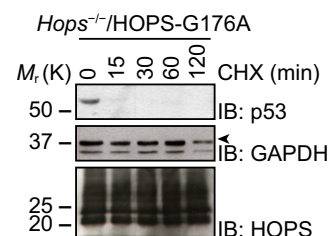


Figure 4.

analysis. Next, we investigated whether HOPS overexpression might affect the p53 binding to importin α in etoposide-treated cells. Co-IP analyses showed a reduction in p53/importin α binding in cells overexpressing HOPS and treated with etoposide (Fig 7C). These data suggest that HOPS competes with importin α in binding to the p53 site that comprises the lysine residues within the 319–321 aa

sequence of the p53 NLS. Post-translational modifications of these residues are known to affect p53 ubiquitination and nuclear import [34]. Consistent with this model, HOPS overexpression significantly decreased the PCAF-mediated acetylation of p53-K320 (Fig 7D), a post-translational modification associated with decreased apoptosis [35,36].

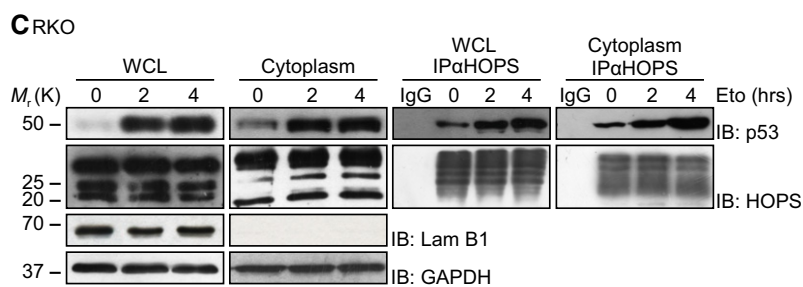
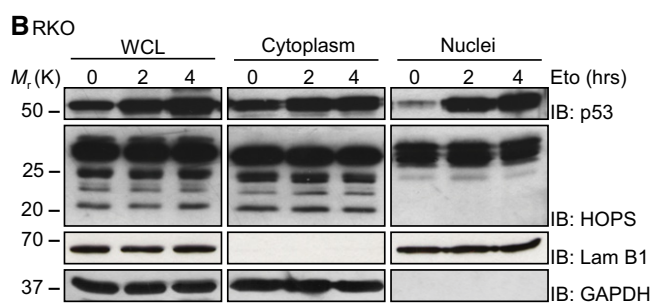
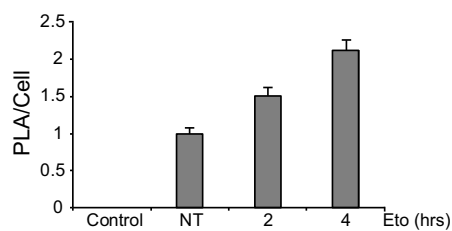
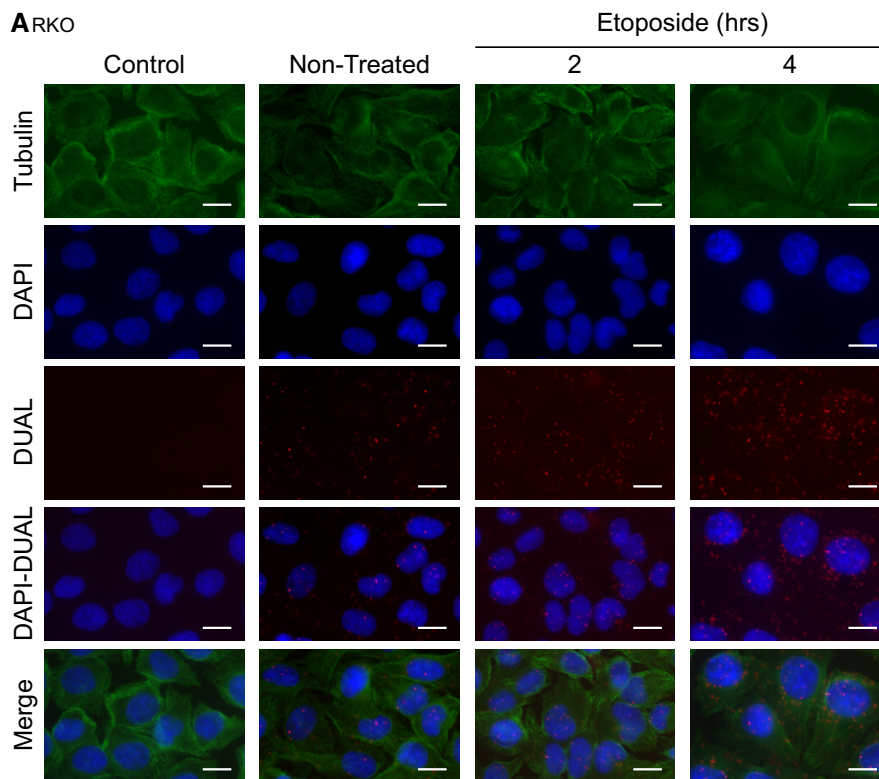


Figure 5.

Figure 5. HOPS binding to p53.

- A Protein binding in RKO cells. PLA showed HOPS/p53 interaction with or without etoposide treatment at the indicated time. Red spots showed a single interaction. DNA counterstaining was performed with DAPI. α -Tubulin-FITC antibody was used to identify the cellular edge. Background control was performed according to the manufacturer's instruction. Scale bars, 10 μ m. The graph represents the binding increase. Non-treated cell binding was assumed as 1.
- B Biochemical analysis of nuclear–cytoplasmic protein distribution. RKO cells were treated with etoposide, collected after 2 and 4 h and processed to obtain nuclear and cytoplasmic fractions. Aliquots relative to the same cell number per fraction were immunoblotted using anti-HOPS and anti-p53 antibodies. GAPDH and Lamin B1 are purity controls of cytoplasmic and nuclear fraction, respectively.
- C HOPS and p53 binding in cytoplasm following apoptosis induction. RKO cells untreated or treated with etoposide as above were used to isolate cytoplasmic fractions. WCL and cytoplasmic fractions were immunoprecipitated with anti-HOPS antibody and subsequently immunoblotted using anti-p53 antibody.
- Data information: All the experiments were performed three times, and representative examples are shown. In (A), data are presented as mean \pm SD.

Discussion

A key hallmark of cancer is the escape from oncosuppressive pathways such as apoptosis, autophagy and cell cycle arrest [9,20]. Loss of apoptotic response by inactivation of the p53 pathway appears to be required for malignant progression [17–20]. In this study, we identified HOPS as a major regulator of cytoplasmic p53 function and fate, in that HOPS is involved in p53 stabilization, p53-mediated mitochondrial apoptosis response and control of p53 nuclear import.

In this regard, we provide insight into HOPS-mediated events that contribute to regulating cytoplasmic p53 apoptosis and levels. After DNA damage, the observed decrease of p53 activation in *Hops*^{-/-} mice prompted us to investigate whether HOPS has a role on p53 regulation. Our findings demonstrate that HOPS is involved in p53 stabilization, as ectopic HOPS prevents p53 proteasomal degradation, and it, in turn, increases p53 protein levels. Depletion of HOPS in *Hops*^{-/-} MEFs results in an increased p53 degradation with a reduced protein half-life. Indeed, the physical interaction between HOPS and p53 results in stabilization of the p53 protein, owing to the presence of a glycine residue in the terminal portion of HOPS UBL domain. Moreover, our data show that following DNA damage, the interaction between HOPS and p53 increases, resulting in p53 translocation to mitochondria to support its apoptotic response. However, the lack of HOPS in mouse significantly reduced the amount of p53 that migrated to mitochondria after DNA damage. Importantly, we provide insight into HOPS-mediated

events that contribute to regulating cytoplasmic p53 levels and function using *in vivo* and *in vitro* models. We found that the association of p53 with HOPS may account for its persistence in the cytoplasm with limited degradation. We showed that in response to DNA damage, the HOPS-bound fraction of cytoplasmic p53 moves to mitochondria, implying that p53, preserved from ubiquitination via HOPS-dependent mechanism, could engage in apoptotic functions.

The accumulation of p53 in the cytoplasm via HOPS binding implies a putative role of HOPS in controlling p53 quantity in cytoplasm. Recently, many studies have pointed to an important role for p53 levels in the cytoplasm [24,25,37]. It has been found that cellular stress promotes a rapid nuclear import of p53, as triggered by an interaction with importin α that takes place within 30 min [34]. Importantly, here, we demonstrate that HOPS not only controls p53 stability, but it interferes with nuclear import by acting on the canonical importin α route. Our data show that the ectopic HOPS expression greatly reduces the p53 binding with importin α that presides over p53 nuclear import. Our findings suggest that within 30 min of application of a stressor, a block occurs in p53 nuclear import due to direct binding with HOPS. The HOPS binding thereby restrains p53 import and further cytoplasmic accumulation for mitochondrial translocation.

Taken together, these data establish an important role for HOPS in regulating mitochondrial apoptosis mediated by p53. More specifically, they clarify the molecular mechanisms whereby p53 accumulates in the cytoplasm defying degradation and nuclear import—all

Figure 6. HOPS, p53 and mitochondria.

- A HOPS localization at mitochondria. RKO cells were stained by MitoTracker™ (red), immediately fixed and stained to visualize HOPS (green). Nuclei were DAPI-stained (blue). Samples were analysed with fluorescent microscope, and representative images were shown. Scale bars, 10 μ m.
- B RKO cells were lysed and processed for mitochondria isolation. WCL, cytoplasm and mitochondria were analysed using anti-HOPS antibody. GAPDH, Lamin B1 and Tom20 are purity controls of mitochondrial fraction.
- C HOPS and p53 translocation to mitochondria. RKO cells were treated with etoposide as indicated and processed for mitochondrial extraction and subsequent immunoblotting for p53, HOPS and the reported extraction purity controls.
- D HOPS/p53 binding at mitochondria. RKO cells were treated with etoposide and subjected to mitochondrial purification, and subsequent immunoprecipitation using anti-HOPS antibody. Samples were immunoblotted to detect p53, HOPS and the reported controls.
- E HOPS and p53 mitochondrial translocation *in vivo*. *Hops*^{+/+} and *Hops*^{-/-} mice were treated with etoposide, and thymus, spleen and testis were harvested. Organs were homogenized, and mitochondrial fraction was isolated and analysed by immunoblotting versus p53. GAPDH and Tom20 are purity controls. p53 mitochondrial protein levels were semi-quantified using Tom20 as loading control, and p53 levels at time 0 were assumed as 1.
- F p53-dependent mitochondrial membrane potential ($\Delta\psi$ m) induction in MEFs. *Hops*^{+/+} and *Hops*^{-/-} MEFs were treated with etoposide and then incubated with JC-1 vital dye. The images were collected by fluorescent microscopy, and representative images are shown (left panel). Scale bars, 10 μ m. Fluorescence was analysed by TECAN plate reader and plotted in the graph (right panel).
- G p53 MOMP induction in HOPS deficiency. Mitochondria from *Hops*^{+/+} and *Hops*^{-/-} MEFs were purified and incubated with p53 recombinant protein. Cytochrome C release from mitochondria as metabolic marker was assayed by immunoblotting. Samples were tested to detect p53 as control and Tom20 as mitochondria structural marker.

Data information: Assays involving animals were performed three times in three different mice per condition. Experiments on mitochondria from MEFs were performed five times. In (E, F), data are presented as mean \pm SD. **P* < 0.05; ****P* < 0.001, by two-tailed Student's *t*-test.

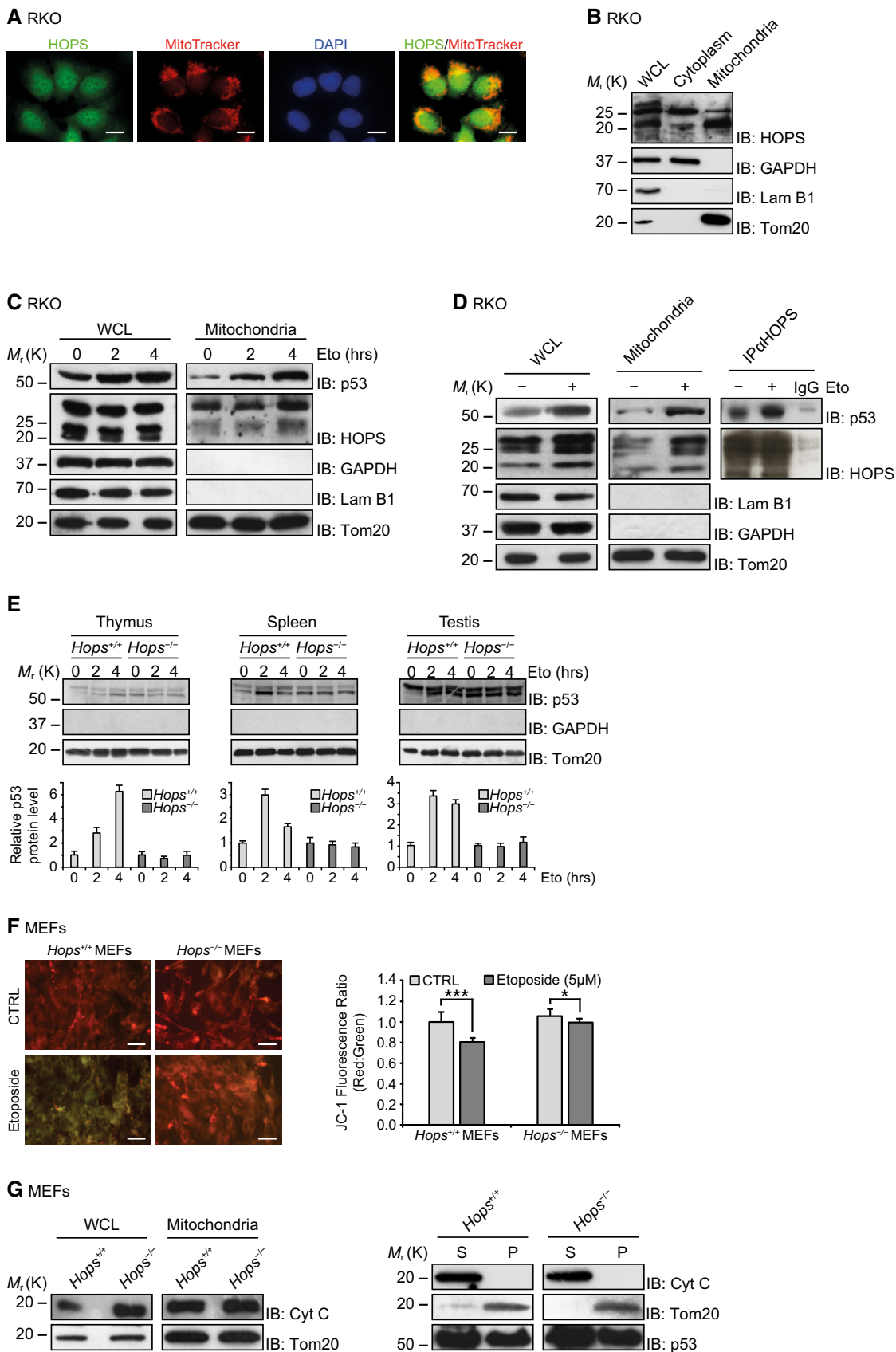
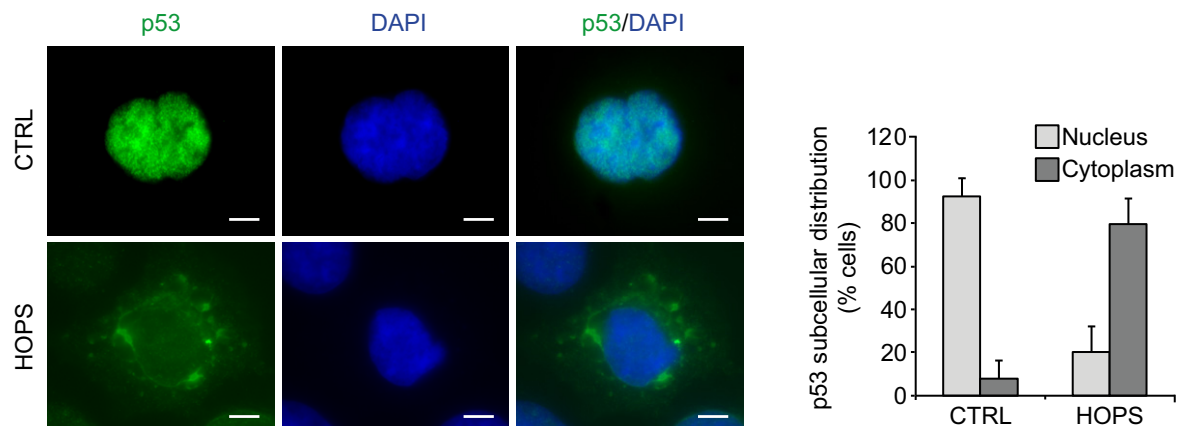


Figure 6.

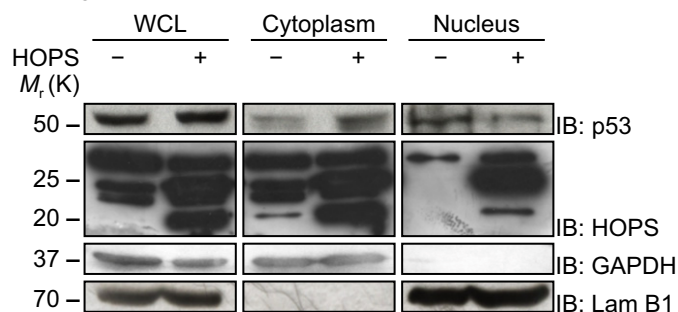
effects involving HOPS—such that HOPS appears to be a p53 modifier and a novel functional partner of p53 in mitochondrial apoptosis.

Recently, it has been demonstrated that increased accumulation of p53 in the cytoplasm is related to an increased malignancy of several human cancers. Furthermore, high level of p53 protein

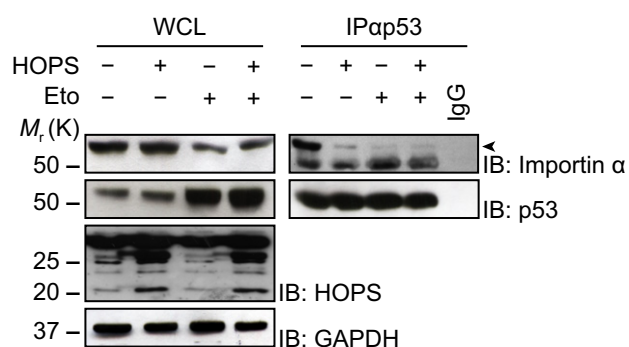
A RKO



B RKO



C RKO



D H1299

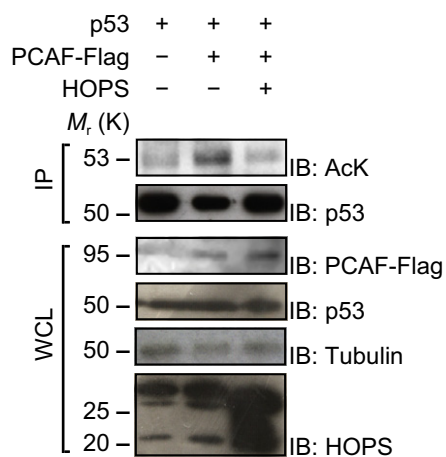


Figure 7.

Figure 7. HOPS role in importin α -mediated p53 nuclear import and PCAF-mediated p53 acetylation.

- A HOPS expression and p53 nuclear accumulation. HOPS was overexpressed in RKO, and cells were fixed and stained with antibody against p53 (green). Nuclei were stained with DAPI (blue). Samples were analysed with fluorescent microscope, and merged images are shown (right panel). Scale bars, 10 μ m. Cells were scored for p53 localization. The results are shown as percentage of nuclear versus cytoplasmic p53 localization in untransfected and HOPS-transfected cells (left panel).
- B Biochemical analysis of HOPS intracellular localization. RKO cells were transfected with HOPS and fractionated into nuclear and cytoplasmic component. Aliquots relative to the same cell number per fraction were immunoblotted using anti-p53 and anti-HOPS antibodies. GAPDH and Lamin B1 are purity controls of cytoplasmic and nuclear fraction, respectively.
- C HOPS and p53 binding to importin α . Untransfected or HOPS-transfected RKO cells were treated with etoposide, and each sample was evaluated by immunoprecipitation with anti-p53 and analysed by immunoblotting using anti-importin α antibody. Arrowhead indicates the importin α specific signal.
- D PCAF-mediated p53 acetylation. p53 and PCAF-Flag-tagged were co-expressed in H1299 cells with or without HOPS and treated with trichostatin A and nicotinamide. p53 acetylation levels were evaluated by immunoprecipitation with anti-p53 antibody followed by immunoblotting with anti-acetylated-Lysine (AcK), anti-p53, anti-Flag, anti-HOPS and anti- α -tubulin antibodies.

Data information: All the experiments detailed above were performed three times, and representative panels are shown. In (A), data are presented as mean \pm SD.

concentration in cytoplasmic has been detected in preneoplastic tissues, and it was linked to cancer transformation [17,24,38]. Many mechanisms may be responsible for the alteration of the proper intracellular compartmentalization of the p53 protein, and an interaction of p53 with HOPS may be one of the major mechanisms. Reinstalling normal localization of p53 is an attractive approach for the treatment of cancer.

Reactivation of tumour p53 in order to trigger apoptosis is a promising approach in cancer therapy [37,39–41]. Thus far, attempts to induce reactivation of the p53 pathway have mostly focused on means of activating the p53 transcriptional programme [42,43]. Yet, the p53 transcriptional response does not necessarily lead to apoptosis, and it may, instead, favour tumour persistence [44,45]. Efforts to activate and regulate cytoplasmic p53 function may, in parallel, lead to the development of alternative strategies of p53-centred anticancer therapy [46–48].

A central finding in our study is the demonstration that HOPS driving of p53 to mitochondria allows an apoptotic response to occur following chemotherapeutic agents. Our finding clearly indicates that HOPS control on p53 may have an *in vivo* relevance by affecting cell susceptibility to DNA damage as induced by drugs. The current study suggests that HOPS, in controlling p53 biology, exerts a potentially important role as a tumour suppressor protein. Interference with regulators of cytoplasmic p53 levels and fate might represent a new tool in anticancer strategies.

Materials and Methods

Generation of *Hops*^{-/-} mouse and treatment

All experiments involving animals were done according to the guidelines of University of Perugia Ethical Committee and the European Communities Council Directive 2010/63/EU. The mice were maintained under specific defined flora/pathogen-free conditions in ventilated (high-efficiency particle-arresting filtered air) sterile microisolator cages at constant temperature (24–26°C), constant humidity (30–50%) and a 12-h light/12-h dark cycle. Sterilized food and tap water were given *ad libitum*.

The *Hops* null mouse was generated by blastocyst injection using gene-targeted embryonic stem (ES) cells produced by Velocigen, Regeneron Pharmaceuticals, Inc. (Tarrytown, NY) for the NIH Knockout Mouse Project (KOMP). The knockout deleted

1,027 bps (23,952,734–23,951,708 of mouse chromosome 5, genome build 37 GRCh37—Genome Reference Consortium) that included the entire *Hops*-coding region. The knockout construct replaced the *Hops* gene in ES cells (C57BL/6NTac background) with a ZEN-UB1 cassette that introduced a bacterial *lacZ* code at the natural *Hops* translation initiation codon (in exon 2) and a downstream neomycin phosphotransferase gene (*neo*^r) driven by the human ubiquitin C gene promoter (*hUBCpro*). The neomycin resistance gene was bracketed by a locus of *X-over P1* sequence from bacteriophage P1 (*loxP*) sequences for convenient removal of the *neo*^r selection code. Successful knockout was determined by PCR genotyping (<http://www.velocigen.com/komp/detail/11654>). The *Tmub1*^{tm1(KOMP)VLcg} (*Hops* locus deletion) allele was genotyped by PCR utilizing primers summarized in Appendix Table S1. All primers were synthesized by Life Technologies (Waltham, MA) and used with GoTaq polymerase (Promega, Madison, WI). The absence of *Hops* mRNA level was revealed by quantitative PCR (qPCR).

For the topoisomerase II inhibitor etoposide (10 mg/kg of body weight; Sigma-Aldrich, St. Louis, MO) treatment, 4- to 5-week-old male *Hops*^{+/+} and *Hops*^{-/-} mice were housed in a pathogen-free barrier area under standard conditions and treated by tail vein injection. No randomization and no blinding of the investigators were used for the experiments on animals. Untreated and treated animals were sacrificed at 0, 2 and 4 h following etoposide treatment by cervical dislocation. Target organs (thymus, spleen, liver and testis) were immediately harvested and either used to touch preparation, embedded in Tissue-Tek[®] O.C.T. Compound (Sakura[®] Finetek, Torrance, CA) for cryosection procedure (5 μ m tissue slide) or washed in ice-cold phosphate-buffered saline (PBS) 1 \times (Sigma-Aldrich, St. Louis, MO) and quickly processed for subcellular fractionation [49].

RNA extraction and Real-time PCR

RNA extraction and real-time PCR were performed as described previously [50]. Total RNA was extracted from cell lines or tissues using TRIzol[®] reagent (Thermo Fisher Scientific, Waltham, MA) according to the manufacturer's instructions. cDNA was reverse-transcribed from 1 μ g of RNA using the iScript kit (Bio-Rad, Hercules, CA). qPCR was performed with SYBR[®] Green qPCR Master Mix (Thermo Fisher Scientific). Primer sequences for *Hops* detection are listed in Appendix Table S1. The relative amount of mRNA was normalized to GUS gene.

Western blot, immunoprecipitation and antibodies

Western blot analysis was performed as previously described [1]. Protein extracts were denatured by adding Laemmli buffer (Tris/HCl at pH 6.8, 200 mM, SDS 8%, bromophenol blue 0.4%, glycerol 40% and β -mercaptoethanol 5%) and boiling for 5 min at 95°C. Protein extracts were normalized by SDS-PAGE followed by Coomassie blue staining. Proteins were separated on polyacrylamide gel (Bio-Rad) and transferred by electroblotting onto nitrocellulose membranes (Bio-Rad). Blots were blocked in dry fat-free milk 5% in PBS 1× for 1 h and then incubated with primary antibody overnight (ON) at 4°C. Detection was achieved using horseradish-peroxidase-conjugated secondary antibody (Bio-Rad) and visualized with ECL (GE Healthcare Life Sciences, Little Chalfont, UK).

For the immunoprecipitation assay, naïve or transfected or treated cells were lysed in RIPA buffer (Tris/HCl at pH 8.0, 50 mM, NaCl 150 mM, SDS 0.1%, sodium deoxycholate 1%, Triton X-100 1%, protease inhibitor cocktail (PIC, Sigma-Aldrich) and 1 mM phenylmethylsulphonyl fluoride (PMSF, Sigma-Aldrich) [1]. Protein lysates were precleared with protein G or A agarose beads (Sigma-Aldrich) for 1 h and then incubated with the specific antibody ON at 4°C. Normal IgG was used as control. Next day, the immunoprecipitated were incubated with protein G or A agarose beads for 2 h at 4°C. Beads were washed three times in RIPA buffer. Protein was eluted from beads with Laemmli buffer, boiled for 5 min and then loaded on polyacrylamide gels for Western blot analysis as described above.

For the detection of human or mouse HOPS were used rabbit polyclonal antibodies produced as described previously [1]. Antibodies against human p53 (DO-1), mouse p53 (A-1), HDM2 (SMP-14), VDAC (FL-283), cytochrome c (7H8) and Tom20 (F-10) were purchased from Santa Cruz Biotechnology (Dallas, TX, USA). Anti-cleaved caspase-3 (Asp175, 5A1E) and anti-acetylated-Lysine were purchased from Cell Signaling Technology. Anti-myc (9E10), anti- α -tubulin (DM 1A), anti-importin α (IM-75), anti-flag (F1804) and anti-GAPDH (G8795) were obtained from Sigma-Aldrich. Anti-Lamin B1 (ab16048) was purchased by Abcam.

Cell culture and treatment

Human epithelial colon carcinoma RKO cells (p53-proficient) were maintained in DMEM containing 10% foetal bovine serum (FBS; EuroClone, Milan, I), and human lung adenocarcinoma H1299 cells (p53-deficient) and lung adenocarcinoma A549 cells (ARF-deficient) were maintained in RPMI 1640 medium containing 10% FBS (EuroClone). The cell lines above described were purchased by ATCC. $p19^{Arf-/-}$ MEFs, $p53^{-/-}$ MEFs and $p53^{-/-}$ $Mdm2^{-/-}$ MEFs were kind gift from P.G. Pelicci and maintained as described previously [7]. All the cell lines were tested for mycoplasma contamination.

$Hops^{+/+}$ MEFs and $Hops^{-/-}$ MEFs were prepared, respectively, from C57BL/6 mice and $Hops^{-/-}$ C57BL/6 mice, and the preparation protocol was adapted from J. Xu [51]. The pregnant mice were sacrificed at 13.5 d.p.c. (day post-coitum) by cervical dislocation. 6–10 embryos can be expected from each pregnant female, and they should yield enough MEFs for several experiments. The embryos were separated from placenta and membranes and placed in 10-cm culture dishes in sterile PBS 1×. Then, liver, heart and brain were

removed and discarded. The remaining part of each embryo was washed and minced with cool razor blade and incubated 20 min at 37°C with trypsin-EDTA 500 mg/l. The minced tissues were chopped by repeated pipetting, then cell suspension was plated in 10-cm tissue culture dishes and 10 ml of DMEM containing 10% FBS (EuroClone) was added. Thymocytes and splenocytes $Hops^{+/+}$ and $Hops^{-/-}$ were prepared from 4- to 6-week-old C57BL/6 mice as previously described [52]. Briefly, thymus and spleen were removed and cut into small pieces and digested with collagenase 100 U/ml. Then, the tissues were recovered in IMDM (Thermo Fisher Scientific) and FBS 10% (EuroClone) and were homogenized prior to a second digestion at 37°C for 30 min with collagenase 400 U/ml. Thymocytes and splenocytes were collected by centrifugation at 270 g for 7 min.

Lipofectamine[®] LTX (Thermo Fisher Scientific) was used to transfect RKO, A549 and MEFs, and Fugene[®]6 (Promega Corporation, Madison, WI, USA) was used to transfect H1299 in accordance with the manufacturer's instructions.

Cells at 80% confluence were treated with 100 μ M cycloheximide (Sigma-Aldrich) for the time points indicated. Proteasome inhibitor MG132 (Merck-Millipore, Darmstadt, D) was applied to cells at 25 μ M for 6 h.

Treatments with etoposide (Sigma-Aldrich) were performed in RKO at 25 μ M, in A549 and MEFs at 5 μ M for the indicated time points. Splenocytes and thymocytes from $Hops^{+/+}$ and $Hops^{-/-}$ mice were processed with etoposide at 1.7 μ M for 2 h. Thymocytes at 80% confluence were treated with 1 μ M dexamethasone (Sigma-Aldrich) for 6 h. Camptothecin (Sigma-Aldrich) was used in MEFs at the indicated concentration for the time points reported.

Apoptosis analysis

For cleaved caspase-3 histological analysis, the slides were blocked with 5% BSA, incubated with specific anti-cleaved caspase-3 antibody (Cell Signaling Technologies, Danvers, MA) and then incubated with Alexa Fluor[®] 488-conjugated goat anti-rabbit IgG (H+L) secondary antibody (Thermo Fisher Scientific). DNA was stained with 4',6-diamidino-2-phenylindole (DAPI, Sigma-Aldrich). Images were captured by fluorescence microscopy as described above. The apoptotic cell number was scored by counting 5 fields 200 cells containing for each group in a random manner.

The apoptosis induced in Thymocytes $Hops^{+/+}$ and $Hops^{-/-}$ or in MEF cells $Hops^{+/+}$ and $Hops^{-/-}$ after treatment with etoposide (5 μ M) or with dexamethasone (1 μ M) for 6 h was measured by flow cytometry. The cells, after treatment, were collected by centrifugation, washed with PBS, stained with Fixable Viability Dye eFluor[®] 780 (eBioscience, CA) for 30 min and then washed with PBS and Flow Cytometry Staining Buffer. 5 μ l of Annexin V conjugated with PerCP-eFluor 710 (eBioscience) was added and incubated with cells at room temperature for 15 min. The percentage of PerCP-eFluor 710 positive apoptotic cells was determined by flow cytometry [53,54].

The study of apoptosis in cells by FACS analysis was also conducted using the Annexin V-FITC Apoptosis Detection Kit (BioVision CA) according to the manufacturer's instructions. Briefly, 2×10^5 cells were added with Annexin V-FITC and propidium iodide and incubated for 5 min at room temperature in the dark, before flow cytometry analysis.

The samples were run on the LSRFortessa flow cytometer (BD Biosciences) and analysed using the FlowJo (Tree Star) analysis software. Each experimental point was performed in triplicates.

The apoptotic cells were detected by using terminal deoxynucleotidyl transferase assay kit (*In Situ* Cell Death Detection Kit Fluorescein, Roche, Basel, CH) which catalyse polymerization of labelled nucleotides to free 3'-OH ends of DNA in a template-dependent manner (TUNEL reaction). Briefly, the tissue section was fixed with 4% paraformaldehyde for 20 min followed by the permeabilization with 0.1% Triton X-100 in 0.1% sodium citrate solution. After washing with PBS 1× (Sigma-Aldrich), TUNEL reaction mixture was added and the slide was then incubated for 60 min at 37°C in the dark in a humidified atmosphere. TUNEL-positive cells were counted using fluorescence microscopy. The apoptotic cell number was scored by counting 5 fields 200 cells containing for each group in a random manner.

Plasmid constructs

The HOPS-coding sequence was amplified and cloned and its cDNA was subcloned in frames with GFP in the pEGFP-N1 expression vector (Clontech Laboratories) as previously described [1,2].

HOPS-G176A and HOPS-K129A mutants were created by site-directed mutagenesis (QuikChange® Site-Directed Mutagenesis Kit, Agilent Technologies, Santa Clara, CA), using *Hops* as template. Constructs coding for human p53 wild-type and mutants were amplified by PCR and cloned in pSCB using StrataClone Blunt PCR Cloning Kit (Agilent Technologies), and then, the constructs were subcloned into appropriate vectors. The appropriate primers used to amplify the specific mutant have been shown in Appendix Table S1. Plasmid encoding His-tagged ubiquitin was kindly provided by D.P. Bohmann, PCAF-Flag tag plasmid was kindly provided by B. Amati and plasmid encoding HDM2 was kind gift by P.G. Pelicci.

In vivo ubiquitin assay

This assay was performed as previously described [55]. Cells were transfected with expressing vector for His-tagged ubiquitin, p53, HDM2 and HOPS or its mutant HOPS-G176A and HOPS-K129A. Cells were treated with MG132 (Sigma-Aldrich) for 6 h at 25 µM prior to harvesting to prevent degradation of ubiquitinated p53. Cells were then lysed in EBC buffer (50 mM Tris-HCl, 120 mM NaCl, 0.5% NP-40) with mild sonication and clarified by centrifugation at 20,000 g for 10 min. Cell lysate (1 mg) was incubated with 30 µl of 50% Ni-NTA His-Bind® Resin (Thermo Fisher Scientific)/EBC slurry for 2 h at 4°C with rotation. The samples were then centrifuged at 10,000 g for 3 min at 4°C, and the supernatant was removed. The Ni-NTA resin was washed several times with 1 ml EBC buffer. His-tagged protein was eluted from the Ni-NTA agarose by incubating in EBC for 5 min at 100°C. The ubiquitinated proteins were analysed by Western blot with a p53-specific antibody.

Fluorescence microscopy

Hepatocyte odd protein shuttling and p53 co-immunofluorescence and HOPS immunofluorescence were performed in RKO cells fixed with 4% paraformaldehyde, permeabilized with Triton X-100 0,2%

and blocked with 3% bovine serum albumin (BSA, Sigma-Aldrich). Cells were stained with anti-HOPS and anti-p53 antibodies. Alexa Fluor® 555-conjugated goat anti-rabbit IgG (H+L) and Alexa Fluor® 488-conjugated goat anti-mouse IgG (H+L) secondary antibodies (Thermo Fisher Scientific) were used. DNA was stained with DAPI (Sigma-Aldrich).

To quantify co-localization of HOPS and p53, we used the Pearson's correlation coefficient (Rr). Cells (200) of selected samples were analysed by using PSC co-localization plug-in (ImageJ-NIH). Rr ranges between -1 (perfect negative correlation) to +1 (perfect positive correlation) with 0 meaning no correlation [56].

For mitochondrial staining, RKO cells were incubated with prewarmed (37°C) growth medium containing MitoTracker™ Red CMXRos (Thermo Fisher Scientific) 50 nM for 30 min. Cells were then fixed with 4% paraformaldehyde for 15 min at 37°C, permeabilized with 0,2% Triton X-100 in PBS 1× and blocked with 3% BSA. Cells were incubated with human anti-HOPS antibody and then incubated with Alexa Fluor® 488-conjugated goat anti-rabbit IgG (H+L) secondary antibody. DNA was stained with DAPI (Sigma-Aldrich).

Images were captured using a Zeiss Axio Observer Z1 inverted microscope, equipped with Apotome filter and AxioCam MRm camera detection system Zeiss. All the images were exported in TIFF, contrast and brightness were adjusted in Corel PaintShop Pro ×9 and final figures were generated with Adobe Illustrator CS6 [57].

Proximity ligation assay

RKO cells, non-treated and after treatment with etoposide at indicated times, were fixed, permeabilized, blocked and stained with anti-HOPS and anti-p53 antibodies as described above. Duolink® (Sigma-Aldrich) was performed, according to the manufacturer's protocol. In brief, PLA probe solution and ligation-ligase solution were added for 1 h and 30 min, respectively. The signal was amplified with amplification polymerase solution at 37°C for 100 min. Then, a counterstain was carried out with using a directly labelled FITC anti-alpha tubulin antibody (Anti-α-Tubulin-FITC antibody, DM 1A Sigma-Aldrich). Nuclei were counterstained with DAPI [58]. Images were captured using a Zeiss Axio Observer Z1 inverted microscope, equipped with Apotome filter and AxioCam MRm camera detection system Zeiss as described above.

HOPS-p53 binding assay *in vitro*

Recombinant p53 His-tagged protein was expressed in *E. coli* BL-21 with IPTG 0.1 mM induction at 30°C. The protein was purified from bacteria through a Ni-NTA His-Bind® Resin (Thermo Fisher Scientific) and eluted by 0.25 M imidazole (Sigma-Aldrich). HOPS protein was produced using TnT® Quick Coupled Transcription/Translation System (Promega). Purified p53 His-tagged protein was incubated with HOPS recombinant protein for 30 min at room temperature in RIPA buffer. Then, the proteins were immunoprecipitated with anti-HOPS antibody and incubated with G-protein beads for 2 h at 4°C. Beads were washed three times in RIPA buffer. Protein was eluted from beads with Laemmli buffer, boiled for 5 min and then loaded onto polyacrylamide gels for Western blot analysis using anti-HOPS and p-53 antibodies.

Nuclear and cytoplasmic fractionation and mitochondrial isolation

Nuclear and cytoplasmic fractions were prepared as previously described [59]. Briefly, RKO cells (5×10^6) were harvested in Extraction Buffer N (Tris-HCl at pH 7.5 15 mM, KCl 60 mM, NaCl 15 mM, MgCl₂ 5 mM, CaCl₂ 1 mM and sucrose 25 mM) supplied with protease inhibitor cocktail (PIC), PMSF (Sigma-Aldrich) and lysed by adding 0.6% of IGEPAL[®] CA-630 (Sigma-Aldrich) following incubation for 1 h at 4°C. Then, the whole-cell lysates (WCL) were centrifuged at 2,000 *g* for 15 min at 4°C. The supernatant (cytoplasm) was removed and conserved, and the pellet (nuclei) was washed twice with Buffer N before to be analysed by Western blot.

The mitochondria from RKO (2×10^6), A549 (2×10^6), *Hops*^{+/+} and *Hops*^{-/-} MEF (1.2×10^7) cells, and splenocytes and thymocytes from *Hops*^{+/+} and *Hops*^{-/-} mice (6×10^7) were isolated using Mitochondria Isolation Kit for Cultured Cells (Thermo Fisher Scientific) according to the instruction manual.

The mitochondria isolation from tissue was performed as previously described with some modifications [60]. *Hops*^{+/+} and *Hops*^{-/-} C57BL/6 mice untreated or treated with etoposide were sacrificed at the reported time by cervical dislocation. Rapidly, thymus, spleen, testis and liver were explanted from each mouse and the tissue was rinsed of blood using cold IBC pH 7.4 (Tris-MOPS 10 mM, Tris-EGTA 1% and sucrose 200 mM). The tissue was minced into small pieces using a scissor, and then, the suspension was harvested with IBC, put in a glass potter, homogenized using Teflon pestle and then centrifuged at 600 *g* for 10 min at 4°C. The supernatant was recovered and centrifuged at 7,000 *g* for 10 min at 4°C. At last, the mitochondrial pellet was washed twice with cold IBC and used for Western blot analysis.

MOMP assay

Release assay for cytochrome c was performed on mitochondria isolated from *Hops*^{+/+} and *Hops*^{-/-} MEFs as previously described with some modifications [61]. Purified mitochondria (350 µg/ml) were incubated with recombinant p53 His-tagged protein (40 nM) for 20 min at 30°C and promptly centrifuged for 5 min at 4°C. Resulting supernatants (S) and washed mitochondrial pellets (P) were analysed by Western blot.

Measurement of the mitochondrial depolarization

Mitochondrial membrane potential has been estimated by using JC1 dye staining (Thermo Fisher Scientific) in accordance with the manufacturer's instructions. Following etoposide treatment, the cells were incubated in JC-1 dye-containing medium (10 µg/ml) for 20 min at 37°. Then, the samples were washed twice with PBS 1× and analysed by fluorescence microscopy or TECAN plate reader. Moreover, after treatment with etoposide the evaluation of the variation of the mitochondrial membrane potential was performed with DiOC6(3) (3,3'-dihexyloxycarbocyanine iodide, Sigma-Aldrich). The cells were trypsinized, and the suspension obtained was adjusted to the density of 1×10^6 /ml and treated with DiOC6 (3) (20 nM) for 15 min at 37°C. The samples were evaluated by flow cytometer.

Determination of acetylated p53 levels

H1299 cells were transfected with p53 or p53/PCAF or p53/PCAF/HOPS. Twenty-four hours after transfection, cells were treated with 10 µM trichostatin A (TSA, Sigma-Aldrich) and 5 mM nicotinamide (NAM, Sigma-Aldrich) for 8 h to prevent deacetylation. Then, the cells were lysed with RIPA buffer containing PIC, 1 mM PMSF, 10 µM TSA and 5 mM NAM with mild sonication. The protein lysates were precleared with G-protein agarose beads for 1 h, and the total p53 immunoprecipitation was performed using anti-p53 antibody (DO-1) ON at 4°C. Next day, the immunoprecipitation was incubated with G-protein agarose beads for 2 h at 4°C. The beads were eluted by Laemmli buffer after being washed with 1 ml of RIPA buffer three times. The samples were further tested by Western blot analysis.

Statistical analysis

The number of mice used was selected on the basis of previous genotyping analyses conducted in the same model and calculating the statistical power of the experiment. Mice were genotyped and according to the genotype assigned to the experimental groups. The information about sample collection, treatment and processing is included in Results and Materials and Methods sections. Data are presented as mean ± SD unless otherwise indicated in figure legends. Sample number (n) indicates the number of independent biological samples in each experiment. Sample numbers and experimental repeats are indicated in figures and figure legends. Statistical analysis between experimental groups was performed using the Student *t*-test or paired *t*-tests. Data analysis was not blinded. Significance levels are **P* < 0.05; ***P* < 0.01; ****P* < 0.001; and n.s., non-significant. *P* value of < 0.05 was considered statistically significant. The chi-square test was performed to determine significant differences between the expected and observed ratios of *Hops*^{-/-} to *Hops*^{+/+} mice. Analyses were performed using the Excel software. The ImageJ software program was used for quantitative densitometric analysis.

Expanded View for this article is available online.

Acknowledgements

We thank Paolo Sassone-Corsi, Karen Voudsen, Pier Giuseppe Pelicci, Fabiola Moretti and Damiano Scopetti for critical reading of the manuscript, materials and insight on the study. We are grateful to Silvano Pagnotta and Maria Luisa Alunni for technical assistance. This study was supported by grants from *Associazione Umbra Contro il Cancro* (AUCC), *Comitato Maria Grazia Frascioni and Fondazione Cassa di Risparmio di Perugia*. G.S. is recipient of a *PRIN Project n.20152CB22L_004*. S. S. is recipient of *AIRC grant n.IG18517*. M.Ca., D.P. and S.P. are recipient of *AUCC fellowship programme*.

Author contributions

MCa, DP, CB, SP, MAD-F and GS jointly conceived the study and designed the experiments. MCa, MCh, DP and CB performed experiments and oversaw the results. MAD-F, DP and MG performed *in vivo* experiments. DP contributed to generate the *Hops* knockout mice and phenotype analysis, contributed *in vivo* experiments, performed statistical analysis and conceptually helped with experiments design. SP contributed ubiquitination assay and biochemical experiments. DB analysed histological specimens and contributed MEFs

preparation. FF and MG provided FACS analysis and contributed *in vivo* assay, and thymocyte and splenocyte preparation. PP reviewed manuscript and discussed data analysis and interpretation. SS reviewed manuscript and gave insight on the study, contributed collective motion analysis and interpretation of the results. MAD-F and GS wrote the paper and directed the study. All authors discussed the results and commented on the manuscript.

Conflict of interest

The authors declare that they have no conflict of interest.

References

- Della Fazia MA, Castelli M, Bartoli D, Pieroni S, Pettirossi V, Piobbico D, Viola-Magni M, Servillo G (2005) HOPS: a novel cAMP-dependent shuttling protein involved in protein synthesis regulation. *J Cell Sci* 118: 3185–3194
- Castelli M, Piobbico D, Bartoli D, Pieroni S, Brunacci C, Bellet MM, Chiacchiarretta M, Della Fazia MA, Servillo G (2014) Different functions of HOPS isoforms in the cell: HOPS shuttling isoform is determined by RIP cleavage system. *Cell Cycle* 13: 293–302
- Yang H, Takagi H, Konishi Y, Ageta H, Ikegami K, Yao I, Sato S, Hatanaka K, Inokuchi K, Seog DH *et al* (2008) Transmembrane and ubiquitin-like domain-containing protein 1 (Tmub1/HOPS) facilitates surface expression of GluR2-containing AMPA receptors. *PLoS One* 3: e2809
- Della Fazia MA, Piobbico D, Bartoli D, Castelli M, Brancorsini S, Viola Magni M, Servillo G (2002) Ial-1: a differentially expressed novel gene during proliferation in liver regeneration and in hepatoma cells. *Genes Cells* 7: 1183–1190
- Zhang W, Savelieva KV, Suwanichkul A, Small DL, Kirkpatrick LL, Xu N, Lanthorn TH, Ye GL (2010) Transmembrane and ubiquitin-like domain containing 1 (Tmub1) regulates locomotor activity and wakefulness in mice and interacts with CAMLG. *PLoS One* 5: e11261
- Pieroni S, Della Fazia MA, Castelli M, Piobbico D, Bartoli D, Brunacci C, Bellet MM, Viola-Magni M, Servillo G (2008) HOPS is an essential constituent of centrosome assembly. *Cell Cycle* 7: 1462–1466
- Castelli M, Pieroni S, Brunacci C, Piobbico D, Bartoli D, Bellet MM, Colombo E, Pelicci PG, Della Fazia MA, Servillo G (2013) Hepatocyte odd protein shuttling (HOPS) is a bridging protein in the nucleophosmin-p19 Arf network. *Oncogene* 32: 3350–3358
- Colombo E, Martinelli P, Zamponi R, Shing DC, Bonetti P, Luzi L, Volorio S, Bernard L, Pruneri G, Alcalay M *et al* (2006) Delocalization and destabilization of the Arf tumor suppressor by the leukemia-associated NPM mutant. *Can Res* 66: 3044–3050
- Vousden KH, Prives C (2009) Blinded by the light: the growing complexity of p53. *Cell* 137: 413–431
- Oren M (2003) Decision making by p53: life, death and cancer. *Cell Death Differ* 10: 431–442
- Brooks CL, Gu W (2010) New insights into p53 activation. *Cell Res* 20: 614–621
- Foulkes WD (2007) p53—master and commander. *N Engl J Med* 357: 2539–2541
- Vogelstein B, Lane D, Levine AJ (2000) Surfing the p53 network. *Nature* 408: 307–310
- Brady CA, Attardi LD (2010) p53 at a glance. *J Cell Sci* 123: 2527–2532
- Vousden KH, Ryan KM (2009) p53 and metabolism. *Nat Rev Cancer* 9: 691–700
- Li T, Kon N, Jiang L, Tan M, Ludwig T, Zhao Y, Baer R, Gu W (2012) Tumor suppression in the absence of p53-mediated cell-cycle arrest, apoptosis, and senescence. *Cell* 149: 1269–1283
- Hollstein M, Sidransky D, Vogelstein B, Harris CC (1991) p53 mutations in human cancers. *Science* 253: 49–53
- Muller PA, Vousden KH (2013) p53 mutations in cancer. *Nat Cell Biol* 15: 2–8
- Goh AM, Coffill CR, Lane DP (2011) The role of mutant p53 in human cancer. *J Pathol* 223: 116–126
- Hanahan D, Weinberg RA (2011) Hallmarks of cancer: the next generation. *Cell* 144: 646–674
- Lakin ND, Jackson SP (1999) Regulation of p53 in response to DNA damage. *Oncogene* 18: 7644–7655
- Fridman JS, Lowe SW (2003) Control of apoptosis by p53. *Oncogene* 22: 9030–9040
- Zilfou JT, Lowe SW (2009) Tumor suppressive functions of p53. *Cold Spring Harb Perspect Biol* 1: a001883
- Comel A, Sorrentino G, Capaci V, Del Sal G (2014) The cytoplasmic side of p53's oncosuppressive activities. *FEBS Lett* 588: 2600–2609
- Marchenko ND, Moll UM (2014) Mitochondrial death functions of p53. *Mol Cell Oncol* 1: e955995
- Mihara M, Erster S, Zaika A, Petrenko O, Chittenden T, Pancoska P, Moll UM (2003) p53 has a direct apoptogenic role at the mitochondria. *Mol Cell* 11: 577–590
- Chipuk JE, Kuwana T, Bouchier-Hayes L, Droin NM, Newmeyer DD, Schuler M, Green DR (2004) Direct activation of Bax by p53 mediates mitochondrial membrane permeabilization and apoptosis. *Science* 303: 1010–1014
- Erster S, Mihara M, Kim RH, Petrenko O, Moll UM (2004) *In vivo* mitochondrial p53 translocation triggers a rapid first wave of cell death in response to DNA damage that can precede p53 target gene activation. *Mol Cell Biol* 24: 6728–6741
- Jamil S, Lam I, Majd M, Tsai SH, Duronio V (2015) Etoposide induces cell death via mitochondrial-dependent actions of p53. *Cancer Cell Int* 15: 79
- Reinhardt HC, Schumacher B (2012) The p53 network: cellular and systemic DNA damage responses in aging and cancer. *Trends Genet* 28: 128–136
- Clarke AR, Purdie CA, Harrison DJ, Morris RG, Bird CC, Hooper ML, Wyllie AH (1993) Thymocyte apoptosis induced by p53-dependent and independent pathways. *Nature* 362: 849–852
- Chen J, Marechal V, Levine AJ (1993) Mapping of the p53 and mdm-2 interaction domains. *Mol Cell Biol* 13: 4107–4114
- Freedman DA, Levine AJ (1998) Nuclear export is required for degradation of endogenous p53 by MDM2 and human papillomavirus E6. *Mol Cell Biol* 18: 7288–7293
- Marchenko ND, Hanel W, Li D, Becker K, Reich N, Moll UM (2010) Stress-mediated nuclear stabilization of p53 is regulated by ubiquitination and importin- α 3 binding. *Cell Death Differ* 17: 255–267
- Chao C, Wu Z, Mazur SJ, Borges H, Rossi M, Lin T, Wang JY, Anderson CW, Appella E, Xu Y (2006) Acetylation of mouse p53 at lysine 317 negatively regulates p53 apoptotic activities after DNA damage. *Mol Cell Biol* 26: 6859–6869
- Brooks CL, Gu W (2011) The impact of acetylation and deacetylation on the p53 pathway. *Protein Cell* 2: 456–462
- Galluzzi L, Morselli E, Kepp O, Tajeddine N, Kroemer G (2008) Targeting p53 to mitochondria for cancer therapy. *Cell Cycle* 7: 1949–1955
- Van Gijssel HE, Ohlson LC, Torndal UB, Mulder GJ, Eriksson LC, Porsch-Hallstrom I, Meerman JH (2000) Loss of nuclear p53 protein in preneoplastic rat hepatocytes is accompanied by Mdm2 and Bcl-2

- overexpression and by defective response to DNA damage *in vivo*. *Hepatology* 32: 701–710
39. Martins CP, Brown-Swigart L, Evan GI (2006) Modeling the therapeutic efficacy of p53 restoration in tumors. *Cell* 127: 1323–1334
 40. Muller PA, Vousden KH (2014) Mutant p53 in cancer: new functions and therapeutic opportunities. *Cancer Cell* 25: 304–317
 41. Kim MP, Zhang Y, Lozano G (2015) Mutant p53: multiple mechanisms define biologic activity in cancer. *Front Oncol* 5: 249
 42. Duffy MJ, Synnott NC, McGowan PM, Crown J, O'Connor D, Gallagher WM (2014) p53 as a target for the treatment of cancer. *Cancer Treat Rev* 40: 1153–1160
 43. Zawacka-Pankau J, Selivanova G (2015) Pharmacological reactivation of p53 as a strategy to treat cancer. *J Intern Med* 277: 248–259
 44. Matt S, Hofmann TG (2016) The DNA damage-induced cell death response: a roadmap to kill cancer cells. *Cell Mol Life Sci* 73: 2829–2850
 45. Shay JW, Roninson IB (2004) Hallmarks of senescence in carcinogenesis and cancer therapy. *Oncogene* 23: 2919–2933
 46. Tal P, Eizenberger S, Cohen E, Goldfinger N, Pietrokovski S, Oren M, Rotter V (2016) Cancer therapeutic approach based on conformational stabilization of mutant p53 protein by small peptides. *Oncotarget* 7: 11817–11837
 47. Soragni A, Janzen DM, Johnson LM, Lindgren AG, Thai-Quynh Nguyen A, Tiourin E, Soriaga AB, Lu J, Jiang L, Faull KF *et al* (2016) A designed inhibitor of p53 aggregation rescues p53 tumor suppression in ovarian carcinomas. *Cancer Cell* 29: 90–103
 48. Oren M, Tal P, Rotter V (2016) Targeting mutant p53 for cancer therapy. *Aging* 8: 1159–1160
 49. Piobbico D, Bartoli D, Pieroni S, De Luca A, Castelli M, Romani L, Servillo G, Della-Fazia MA (2018) Role of IL-17RA in the proliferative priming of hepatocytes in liver regeneration. *Cell Cycle* 17: 2423–2435
 50. Bellet MM, Piobbico D, Bartoli D, Castelli M, Pieroni S, Brunacci C, Chiacchiarretta M, Del Sordo R, Fallarino F, Sidoni A *et al* (2014) NEDD4 controls the expression of GUCD1, a protein upregulated in proliferating liver cells. *Cell Cycle* 13: 1902–1911
 51. Xu J (2005) Preparation, culture, and immortalization of mouse embryonic fibroblasts. *Curr Protoc Mol Biol* Chapter 28: Unit 28 1
 52. Fallarino F, Grohmann U, Vacca C, Bianchi R, Orabona C, Spreca A, Fioretti MC, Puccetti P (2002) T cell apoptosis by tryptophan catabolism. *Cell Death Differ* 9: 1069–1077
 53. Pucciarini L, Ianni F, Petesse V, Pellati F, Brighenti V, Volpi C, Gargaro M, Natalini B, Clementi C, Sardella R (2019) Onion (*Allium cepa* L.) skin: a rich resource of biomolecules for the sustainable production of colored biofunctional textiles. *Molecules* 24: E634
 54. Romani R, Pirisinu I, Calvitti M, Pallotta MT, Gargaro M, Bistoni G, Vacca C, Di Michele A, Orabona C, Rosati J *et al* (2015) Stem cells from human amniotic fluid exert immunoregulatory function via secreted indoleamine 2,3-dioxygenase1. *J Cell Mol Med* 19: 1593–1605
 55. Li M, Brooks CL, Wu-Baer F, Chen D, Baer R, Gu W (2003) Mono- versus polyubiquitination: differential control of p53 fate by Mdm2. *Science* 302: 1972–1975
 56. French AP, Mills S, Swarup R, Bennett MJ, Pridmore TP (2008) Colocalization of fluorescent markers in confocal microscope images of plant cells. *Nat Protoc* 3: 619–628
 57. Bartoli D, Piobbico D, Bellet MM, Bennati AM, Roberti R, Della Fazio MA, Servillo G (2016) Impaired cell proliferation in regenerating liver of 3 beta-hydroxysterol Delta14-reductase (TM7SF2) knock-out mice. *Cell Cycle* 15: 2164–2173
 58. Choi S, Chen M, Cryns VL, Anderson RA (2019) A nuclear phosphoinositide kinase complex regulates p53. *Nat Cell Biol* 21: 462–475
 59. Remboutsika E, Lutz Y, Gansmuller A, Vonesch JL, Losson R, Chambon P (1999) The putative nuclear receptor mediator TIF1alpha is tightly associated with euchromatin. *J Cell Sci* 112(Pt. 11): 1671–1683
 60. Frezza C, Cipolat S, Scorrano L (2007) Organelle isolation: functional mitochondria from mouse liver, muscle and cultured fibroblasts. *Nat Protoc* 2: 287–295
 61. Wolff S, Erster S, Palacios G, Moll UM (2008) p53's mitochondrial translocation and MOMP action is independent of Puma and Bax and severely disrupts mitochondrial membrane integrity. *Cell Res* 18: 733–744